Applied Mathematical Modelling 77 (2020) 1936–1953

Contents lists available at ScienceDirect

Applied Mathematical Modelling

journal homepage: www.elsevier.com/locate/apm

Analysis of melting behavior of PCMs in a cavity subject to a non-uniform magnetic field using a moving grid technique

Mohammad Ghalambaz[a,*], Seyed Mohsen Hashem Zadeh[b], S.A.M. Mehryan[c], Ioan Pop[d], Dongsheng Wen[a,e,*]

[a] School of Aeronautic Science and Engineering, Beihang University, Beijing, PR China
[b] Department of Mechanical Engineering, Shahid Chamran University of Ahvaz, Iran
[c] Young Researchers and Elite Club, Yasooj Branch, Islamic Azad University, Yasooj, Iran
[d] Department of Mathematics, Babeş-Bolyai University, 400084 Cluj-Napoca, Romania
[e] School of Chemical and Process Engineering, University of Leeds, Leeds, UK

ARTICLE INFO

Article history:
Received 23 March 2019
Revised 25 July 2019
Accepted 3 September 2019
Available online 9 September 2019

Keywords:
Non-uniform magnetic field
Line-source magnet
Melting heat transfer
Phase change heat transfer
Moving mesh method

ABSTRACT

Melting flow and heat transfer of electrically conductive phase change materials subjecting to a non-uniform magnetic field are addressed in a square enclosure. The top and bottom walls of the cavity are adiabatic, and the sidewalls are isothermal at different temperatures. The temperature of the hot wall is higher than the fusion temperature of PCM (T_f), and the cold wall is at the fusion temperature or lower. At the initial time, the cavity is filled with a solid saturated PCM. In the vicinity to the hot wall, there is an external line-source magnet, inducing a magnetic field. The location of the magnetic source (Y_0) can be changed along the hot wall. The cavity domain is divided into two parts of the liquid domain and the solid domain. The moving grid method is utilized to track the phase change interface at the exact fusion temperature of T_f. The governing equations for continuity, flow and heat transfer associated with the Arbitrary Lagrangian–Eulerian (ALE) moving mesh technique are solved using the finite element method. The results are investigated for the melting behavior of PCM by the study of Hartmann number ($0 \le Ha \le 50$) and the location of the magnetic source ($0 \le Y_0 \le 1$). Outcomes show that the effect of the magnetic field on the melting behavior of PCM is negligible at the initial stages of the melting ($Fo < 1.15$). However, after the initial stages of the melting, the effect of the presence of a magnetic field becomes significant. Moreover, the location of the magnetic source induces a feeble effect on the melting front at the initial melting stages, but its effect on the shape of the melting front increases by the increase of the non-dimensional time. The location of the magnetic source also significantly affects the streamlines patterns. Changing the position of the magnetic source from the bottom of the cavity ($Y_0 = 0.2$) to the almost middle of the cavity ($Y_0 = 0.6$) would decrease the required non-dimensional time of full melting from $Fo = 10.4$ to $Fo = 9.0$.

1. Introduction

The Phase Change Materials (PCMs) are capable of storing or releasing a large amount of latent energy during solidification or melting. Therefore, PCMs have been subject of various practical applications in the body of domestic buildings

* Corresponding authors at: School of Aeronautic Science and Engineering, Beihang University, Beijing, PR China.
E-mail addresses: m.ghalambaz@iaud.ac.ir (M. Ghalambaz), d.wen@buaa.edu.cn (D. Wen).

https://doi.org/10.1016/j.apm.2019.09.015
0307-904X/

Nomenclature

B	magnetic induction vector
c_p	specific heat in constant pressure (J/kg °C)
Ec	Eckert number
$\boldsymbol{F}$	volumetric force (N/m^3)
Fo	non-dimensional time (Fourier number)
g	gravitational acceleration (m/s^2)
H	the strength of the magnetic field
Ha	Hartmann number
$\boldsymbol{J}$	voltage field (V)
k	thermal conductivity coefficient (W/mK)
L	cavity size
P	pressure (Pa)
Pr	Prandtl number
$\boldsymbol{Q}$	Joule heating source term
Ra	Rayleigh number
S	dimensionless stream function
Ste	Stefan number
t	time (s)
T	temperature (°C)
$\boldsymbol{u}$	velocity (m/s)
u	velocity component in the x-direction (m/s)
U	non-dimensional velocity component in the x-direction
v	velocity component in the y-direction (m/s)
V	non-dimensional velocity component in the y-direction
x	Cartesian coordinate in the horizontal direction (m)
X	non-dimensional Cartesian coordinate in the horizontal direction
y	Cartesian coordinate in the vertical direction (m)
Y	the non-dimensional Cartesian coordinate in the vertical direction

Greek symbols

μ	dynamic viscosity (kg s/m)
$\mu 0$	magnetic constant
α	thermal diffusivity (m^2/s)
β	thermal expansion coefficient (1/K)
γ	the strength of the magnetic source
θ	non-dimensional temperature
ρ	density (kg/m^3)
σ	the electrical conductivity of the liquid (Ω m)

Subscript

0	location of the magnetic source
B	buoyancy force
c	cold
f	fusion
h	hot
L	Lorentz force
l	liquid
s	solid

Superscript

*	dimensional values

and building envelopes such as walls, roofs, ceilings, and floors [1,2]. Moreover, PCMs have found applications for thermal energy storage in concentrated solar thermal power plants [3]. In thermal storage applications, PCMs are packed in solid flat plates, solid cylinders, spheres, rods and various forms of enclosures [4–7]. Farah and Farouk [8] studied some practical applications of using PCMs in energy storage systems.

By using PCMs, the renewable sources of energy can be stored in the form of the latent heat of phase change if the time of demand does not coincide with the time of production. In fact, the amount of latent heat that can be stored in a

unit volume of a PCM is much larger than that of the sensible heat. Hence, a large amount of energy can be stored in the form of phase change latent heat. Fokaides et al. [9] and Silva et al. [10] reviewed the application of phase change materials in transparent elements for buildings usage. The transparent PCMs have found essential applications in windows cavities, decorated walls, and light walls.

Tay et al. [11] point out one of the very important advantages of PCMs thermal storage for time shift of energy usage. PCMs can be charged in off-peak electricity tariffs with low-cost electricity and later be used as a heating or cooling source in regular times. Malik et al. [12] studied the application of PCMs in battery thermal management for electric and hybrid electric vehicles. Chandel and Agarwal [13] reviewed the application of PCMs as energy storage coolants for enhancing the efficiency of photovoltaic power systems. The literature review shows that PCMs are packed and contained in closed enclosure units. In this regard, Kylili and Fokaides [14] performed a review study on numerical analysis of PCMs in cavity enclosures. Due to the importance of natural convection heat transfer in enclosures, this phenomenon has been addressed in many of the recent studies such as Alsabery et al. [15,16], Janagi et al. [17], Pop et al. [18], Zargartalebi et al. [19], and Sheikholeslami [20,21].

The magnetic field can be the result of high-power transformers, current in batteries or microwave systems with a transient electrical load. In such systems, a phase change heatsink can be utilized for thermal management of the device in environments with low ventilation. The heatsink is the cavity enclosure with a potential of energy storage/release and the magnetic field is the device. A magnetic field can affect the convective heat transfer in an enclosure as a controlling mean for control of heat transfer rate. Considering the presence of a magnetic field, most of the available works have addressed the effect of the presence of a uniform or an inclined uniform magnetic field on the single-phase convection applications with no phase change. The presence of a uniform magnetic field induces volumetric forces on the moving electrical conducting fluid proportional to the fluid velocity. For example, in the case of natural convection of a liquid fluid (with no phase change), Rashad et al. [22] investigated the entropy generation and heat transfer in an inclined cavity subject to a uniform magnetic field. Dogonchi et al. [23] conducted the numerical analysis of natural convection inside in the cavity containing inclined elliptical heater under shape factor of nanoparticles and magnetic field. Also, the natural convection heat transfer in a square enclosure with a wavy circular heater under magnetic field is studied by Dogonchi et al. [24]. Chamkha and Selimefendigil [25] investigated the Magnetohydrodynamic natural convection and entropy generation in a corrugated porous cavity using finite element method. Sheremet et al. [26] addressed the effect of magnetic field on the flow and heat transfer of nanofluids in a cavity filled with a porous media. Reddy and Murugesan [27] analyzed the influence of an inclined uniform magnetic field on the double-diffusive natural convection in a square cavity with the temperature difference at the vertical walls. The outcomes reveal that the increase of the magnetic-field-intensity decreases the heat and mass transfer in the cavity.

Considering the melting and an inclined uniform magnetic field effect, Bondareva and Sheremet [28] addressed the melting heat transfer in a 2D square cavity subject to a uniform magnetic field. The vertical walls were at a constant cold temperature, and there was a constant temperature heat source at the bottom of the cavity. The other parts of the cavity walls were well insulated. At the initial time, the cavity was filled with a solid phase change material. Later, PCM started to phase change from the solid to liquid due to the energy of the heat source. The results showed that a symmetrical thermo-hydrodynamic structure was observed in the liquid at the beginning of the melting. The structure of this initial region is not under the influence of the magnetic field. However, as the molten region around the heat source starts to extend, the effect of the magnetic field becomes significant. The inclination angle of the magnetic field tends to reduce the symmetry of the molten zone.

Later, Bondareva and Sheremet [29] extended their previous work presented in [28] to the case of a 3D cavity. They investigated the effect of an inclined uniform magnetic field on the melting heat transfer of gallium in a 3D cubic cavity. They studied a cavity bounded by two opposite isothermal cold vertical-walls while the other cavity walls were well insulated. There was a heat source with constant hot temperature, mounted at the bottom of the cavity. At the initial state, the gallium in the cavity was in a solid phase. So that, the melting commenced from the below of the cavity due to the energy of the heat source. The results show that the increase in the intensity of the magnetic field reduces the convective heat transfer. For large values of the magnetic field, the natural convection can be suppressed, which leads to a stratified liquid around the heat source. Sheikholeslami and Rokni [30] investigated the melting behavior of CuO–water nanofluid in a cavity in the presence of an inclined uniform magnetic field.

The uniform magnetic field can be produced as the result of a solenoid magnetic field. However, there are many cases, in which the magnetic field is variable in space. For example, the magnetic field around a wire is variable with the distance from the wire. The non-uniform magnetic field, induced by a line magnetic source, has been addressed in some of the recent studies regarding the natural convective heat transfer in cavities with no phase-change heat transfer. Sheikholeslami et al. have addressed the effect of a point source magnetic field on the flow and heat transfer of Fe_3O_4–water nanofluid in a semi-annulus enclosure [31], a lid-driven semi annulus enclosure [32], a semi-rectangle enclosure [33] and circular cavity [34]. The outcomes show that the presence of the magnetic field decreases the heat transfer rate. Later, some researchers studied the natural convection heat transfer of nanofluids in a square cavity [35], a cavity with a hot pipe [36] and a wavy wall cavity [37] in the presence of a non-uniform magnetic field. These authors [35–37] studied the effect of Rayleigh and Hartmann numbers on flow and heat transfer of Fe_3O_4–water nanofluid. The results show that the heat transfer is a decreasing function of the Lorentz force.

From the theoretical point of view, the modeling of phase-change heat transfer in enclosures has been subject of two major approaches, the enthalpy-porosity methods and the phase change interface tracking methods. In the enthalpy-porosity method, it is assumed that the phase change occurs in a temperature range instead of an exact fusion temperature. So, the latent heat of phase change is included in the heat capacity of the phase-change medium. The momentum equation in liquid and solid regions is controlled by using source terms. The source terms affect the momentum in a way to allow free fluid motion in liquid regions, but they force the velocity to zero in solid regions. It should be noted that dealing with a temperature range instead of an exact fusion temperature is a modeling approximation which adds some modeling errors. This approximation error can be overcome by reducing the fusion temperature range; however, a narrow fusion temperature range results in some instability and convergence problems. Besides, a very high grid resolution is also required to capture the temperature gradients at the phase change interface.

Another approach to model the phase-change is dividing the domain of the solution into pure solid and pure liquid phases, and hence, the phase change can occur at the interface of the two regions at an exact fusion temperature. In this approach, the solid region shrinks and the liquid region expands as the melting process continues in time. Thus, an interface tracking system is required to follow the melting interface. Viswanath and Jaluria [38], Wintruff et al. [39] and Li et al. [40] discussed the advantage and drawbacks of these solution methods in details.

Considering the enthalpy-porosity method, Sushobhan and Kar [41] studied the melting of nano-based phase change materials in a cavity for the applications of thermal energy storage. Yang et al. [42] analyzed the melting of gallium in a cavity with a temperature difference between the vertical walls. Ye [43] investigated the effect of the cavity aspect ratio on the melting behavior of phase change materials. The vertical walls of the cavity were subject to in isothermal hot temperature, and the top and bottom walls were adiabatic. The outcomes reveal that the aspect ratios significantly affect the time scale of melting phenomenon and the structure of the convection currents inside the cavity. Bondareva and Sheremet [28,29] utilized the enthalpy-porosity method differently. They solved the momentum equations solely in grid cells with liquid, and they considered the cells with the solid as the boundaries for momentum equations. This way, they do not need to deal with source teams and convergence problems. However, this method has some drawbacks. For example, criteria for deciding the cell is solid or liquid are required. In every time step, the grid domain for momentum equations should be updated. In contrast, Hossain et al. [44] and Al-Jethelah et al. [45] utilized an interface tracking approach to model the melting flow and heat transfer in a porous space.

The literature review shows that the non-uniform magnetic field has been studied in enclosures with single phase natural convective heat transfer in recent years. The uniform melting heat transfer (two-phase) has also been investigated in the literature. However, the effect of the line-source magnetic field on the melting heat transfer has not been addressed yet. To the best of the author's knowledge, the present study is the first work to analyze the effects of the presence and location of a non-uniform magnetic source on the melting rate of an MHD phase change material utilizing advanced tracking method (moving grid method).

2. Mathematical model

Fig. 1 illustrates the schematic view of the domain of interest selected for this study. A phase-change solid substance with initial temperature T_f has filled the enclosure. As can be seen in Fig. 1, the right wall and the left wall are in the hot and the cold isothermal temperatures of T_h and T_c, respectively. The top and bottom bounds are well insulated. There is a magnetic source at the location of (x_0, y_0) outside the cavity. The intensity of the magnetic source is variable and decreases as the square of the distance with the source. The gravity and non-uniform magnetic body forces influence the entire of the enclosure domain. Due to the thermal buoyancy effects, there is a natural convection flow in the molten region. It is assumed that the thermo-physical properties in the molten and solid regions are independent of temperature except for the density which is modeled by the Boussinesq approximation. It is also assumed that the flow of the melted substance is laminar and Newtonian.

Following the studies of Sheikholeslami et al. [31] and Sheikholeslami and Vajravelu [35], and the components of the intensity of the magnetic field along x and y axes introduced by H_x^* and H_y^*, respectively. The strength of the magnetic field, H^*, can be written as follow:

$$H_x^* = \frac{\gamma}{2\pi}\frac{(y-y_0)}{(x-x_0)^2+(y-y_0)^2} \tag{1-a}$$

$$H_y^* = -\frac{\gamma}{2\pi}\frac{(x-x_0)}{(x-x_0)^2+(y-y_0)^2} \tag{1-b}$$

$$H^* = \left(H_x^{*^2} + H_y^{*^2}\right)^{0.5} \tag{1-c}$$

In the relations introducing the magnetic field, γ is the strength of the magnetic source in (x_0, y_0). Applying the above assumptions to derive the governing equations leads to the equations given below:

Continuity equation:

$$\nabla \cdot \boldsymbol{u} = 0 \tag{2}$$

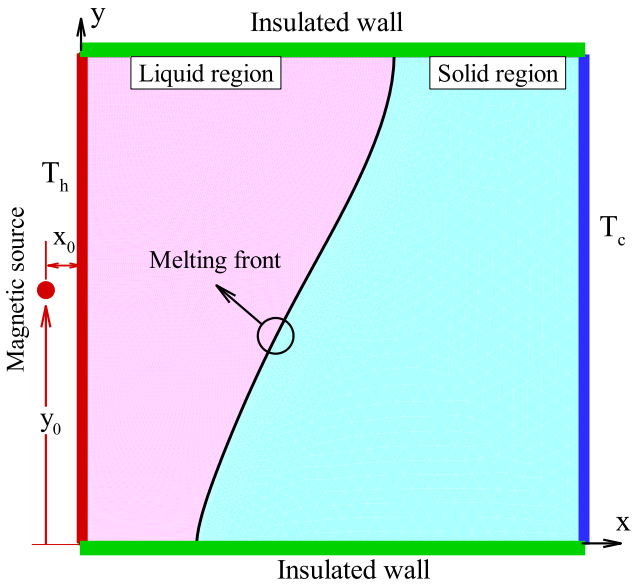

Fig. 1. Schematic view of the physical model and computational domain.

where $\boldsymbol{u}$ is the velocity vector including u and v components along x and y directions.

Momentum equation:

$$\rho\left(\frac{\partial \boldsymbol{u}}{\partial t}+\boldsymbol{u}\cdot\nabla\boldsymbol{u}\right)=-\nabla p+\mu\nabla^2\boldsymbol{u}+\boldsymbol{F} \tag{3}$$

In this equation, $\boldsymbol{F}$, the volume force, can be explained as follow

$$\boldsymbol{F}=\boldsymbol{F_L}+\boldsymbol{F_B} \tag{4}$$

where $\boldsymbol{F_L}$ is Lorentz force that is related to the velocity field so that $\boldsymbol{F_L}=\boldsymbol{J}\times\boldsymbol{B}$. Here $\boldsymbol{B}$ is the magnetic induction vector with components of $B_x=\mu_0 H_x^*$ and $B_y=\mu_0 H_y^*$. $\boldsymbol{J}$ is also the voltage field. Three vectors of the magnetic induction, velocity and voltage are correlated by the equation given below:

$$\boldsymbol{J}=\sigma\left(-\nabla\phi+\boldsymbol{u}\times\boldsymbol{B}\right) \tag{5}$$

The buoyancy force applied to the flow field is $\boldsymbol{F_B}$ and is written as:

$$\boldsymbol{F_B}=\rho g\beta\left(T-T_f\right) \tag{6}$$

Energy equation of liquid PCM:

$$(\rho c_p)_l\left(\frac{\partial T}{\partial t}+\boldsymbol{u}.\nabla T\right)=k_l\nabla^2 T+Q \tag{7}$$

The magnetic field can lead to heat generation Q as known joule heating:

$$Q=\sigma\left(uB_y-vB_x\right)^2 \tag{8}$$

Energy equation of solid PCM:

$$(\rho c_p)_s\frac{\partial T}{\partial t}=k_s\nabla^2 T \tag{9}$$

The boundary conditions of the domain are presented as:

$$x=0, 0\le y\le L, t>0\rightarrow u=v=0, T=T_h \tag{10-a}$$

$$x=L, 0\le y\le L, t>0\rightarrow u=v=0, T=T_c \tag{10-b}$$

$$y=0, 0\le x\le L, t>0\rightarrow u=v=0, \partial T/\partial y=0 \tag{10-c}$$

$$y=L, 0\le x\le L, t>0\rightarrow u=v=0, \partial T/\partial y=0 \tag{10-d}$$

$$t = 0, 0 \le x \le L, 0 \le y \le L, t > 0 \rightarrow u = v = 0, T = T_f \tag{10-e}$$

In order to evaluate the displacement velocity, and hence, the grid movement of the interface, the interfacial energy balance or Stefan condition is utilized:

$$k_l \left.\frac{\partial T}{\partial x}\right|_l - k_s \left.\frac{\partial T}{\partial x}\right|_s = \rho u h_{sf} \tag{11-a}$$

$$k_l \left.\frac{\partial T}{\partial y}\right|_l - k_s \left.\frac{\partial T}{\partial y}\right|_s = \rho v h_{sf} \tag{11-b}$$

The dimensionless parameters, introduced as below, are employed to transfer the dimensional equations to dimensionless X–Y coordinates:

$$X = \frac{x}{L}, Y = \frac{y}{L}, U = \frac{uL}{\alpha_l}, V = \frac{vL}{\alpha_l}, \theta = \frac{T - T_c}{T_h - T_c}, P = \frac{L^2 p}{\rho {\alpha_l}^2},$$
$$H = \frac{H^*}{H_0^*}, H_X = \frac{H_x^*}{H_0^*}, H_Y = \frac{H_y^*}{H_0^*}, Fo = \frac{t\alpha_l}{L^2} \tag{12}$$

where $H_0^* = \gamma / 2\pi L$. Substituting these parameters for the governing equations result in the appearance of the following dimensionless equations:

$$\frac{\partial U}{\partial X} + \frac{\partial V}{\partial Y} = 0 \tag{13}$$

$$\frac{\partial U}{\partial Fo} + U\frac{\partial U}{\partial X} + V\frac{\partial U}{\partial Y} = -\frac{\partial P}{\partial X} + Pr\left(\frac{\partial^2 U}{\partial X^2} + \frac{\partial^2 U}{\partial Y^2}\right) - Ha^2 Pr H_Y (UH_Y - VH_X) \tag{14}$$

$$\frac{\partial V}{\partial Fo} + U\frac{\partial V}{\partial X} + V\frac{\partial V}{\partial Y} = -\frac{\partial P}{\partial Y} + Pr\left(\frac{\partial^2 V}{\partial X^2} + \frac{\partial^2 V}{\partial Y^2}\right) - Ha^2 Pr H_X (VH_X - UH_Y) + RaPr\theta \tag{15}$$

$$\frac{\partial \theta}{\partial Fo} + U\frac{\partial \theta}{\partial X} + V\frac{\partial \theta}{\partial Y} = \left(\frac{\partial^2 \theta}{\partial X^2} + \frac{\partial^2 \theta}{\partial Y^2}\right) + EcHa^2 (UH_Y - VH_X)^2 \tag{16}$$

$$\frac{\partial \theta}{\partial Fo} = \left(\frac{\partial^2 \theta}{\partial X^2} + \frac{\partial^2 \theta}{\partial Y^2}\right) \tag{17}$$

where

$$Ra = \frac{g\beta\left(T_h - T_f\right)L^3}{\mu_l \alpha_l}, Pr = \frac{\upsilon}{\alpha_l}, Ha = \mu_0 H_0 L\sqrt{\frac{\sigma_l}{\mu_l}},$$
$$Ec = \frac{\mu_l \alpha_l}{\rho_l c_{p,l}\left(T_h - T_f\right)L^2}, Ste = \frac{h_{sf}\left(T_h - T_f\right)}{k_l} \tag{18}$$

The boundary conditions in dimensionless coordinates X–Y are:

$$X = 0, 0 \le Y \le 1, Fo > 0 \rightarrow U = V = 0, \theta = 1 \tag{19-a}$$

$$X = 1, 0 \le Y \le 1, Fo > 0 \rightarrow U = V = 0, \theta = \left(T_c - T_f\right)/\left(T_h - T_f\right) \tag{19-b}$$

$$Y = 0, 0 \le X \le 1, Fo > 0 \rightarrow U = V = 0, \partial\theta/\partial Y = 0 \tag{19-c}$$

$$Y = 1, 0 \le X \le 1, Fo > 0 \rightarrow U = V = 0, \partial\theta/\partial Y = 0 \tag{19-d}$$

$$Fo = 0, 0 \le X \le 1, 0 \le Y \le 1 \rightarrow U = V = 0, \theta = 0 \tag{19-e}$$

Here, it is assumed that T_c=T_f, and hence, θ=0 at X=1. Besides, the dimensionless equations of movement of the solid–liquid interface can be written as

$$U = Ste\left(\left.\frac{\partial\theta}{\partial X}\right|_l - \left.\frac{\partial\theta}{\partial X}\right|_s \right) \tag{20-a}$$

$$V = Ste\left(\left.\frac{\partial\theta}{\partial Y}\right|_l - \left.\frac{\partial\theta}{\partial Y}\right|_s \right) \tag{20-b}$$

The moving grid method requires an initial small region of liquid to be defined as the liquid region. Hence, at the initial state, one percent of the length of the cavity is assumed in the melting phase with an initial non-dimensional temperature of zero. This assumption is required for dividing of the cavity into two domains of liquid and solid and commencing of the melting process.

3. Numerical approach

To solve the coupled and non-linear Eqs. (13)–(17) and the boundary conditions of Eqs. (19) and (20), the Galerkin finite element method is employed. The details of this method are well discussed in [46,47]. The pressure term in momentum equations can be eliminated by a penalty function defined as follows:

$$P = \chi\left(\frac{\partial U}{\partial X} + \frac{\partial V}{\partial Y}\right) \tag{21}$$

It is known that the continuity equation is satisfied, if χ, namely penalty number, is a large value. Substituting this penalty function for pressure term gives the following equations:

$$\frac{\partial U}{\partial Fo} + U\frac{\partial U}{\partial X} + V\frac{\partial U}{\partial Y} = -\frac{\partial}{\partial X}\left(\chi\left(\frac{\partial U}{\partial X} + \frac{\partial V}{\partial Y}\right)\right) + Pr\left(\frac{\partial^2 U}{\partial X^2} + \frac{\partial^2 U}{\partial Y^2}\right) - Ha^2 PrH_Y(UH_Y - VH_X) \tag{22}$$

$$\frac{\partial V}{\partial Fo} + U\frac{\partial V}{\partial X} + V\frac{\partial V}{\partial Y} = -\frac{\partial}{\partial Y}\left(\chi\left(\frac{\partial U}{\partial X} + \frac{\partial V}{\partial Y}\right)\right) + Pr\left(\frac{\partial^2 V}{\partial X^2} + \frac{\partial^2 V}{\partial Y^2}\right) - Ha^2 PrH_X(VH_X - UH_Y) + RaPr\theta \tag{23}$$

Employing a basis set $\{\xi_k\}_{k=1}^N$, the velocity components, and the temperature can be expanded such as:

$$U \approx \sum_{k=1}^{N} U_k\xi_k(X,\ Y), V \approx \sum_{k=1}^{N} V_k\xi_k(X,\ Y),\ \theta \approx \sum_{k=1}^{N} \theta_k\xi_k(X,\ Y) \tag{24}$$

Since the basic functions of the variables ξ are the same, the total grids number for all of the variables is $N=3$. The heat and fluid equations were coupled using the Newton method, and they were solved simultaneously using a MUltifrontal Massively Parallel Sparse (MUMPS) direct solver [48,49]. The use of Galerkin finite element approach results in the non-linear residuals as below:

$$\begin{aligned} R_i^1 \approx{}& \sum_{k=1}^{N} U_k \int \frac{\partial\xi_k}{\partial Fo}\xi_i dXdY + \sum_{k=1}^{N} U_k \int \left[\left(\sum_{k=1}^{N} U_k\xi_k\right)\frac{\partial\xi_k}{\partial X} + \left(\sum_{k=1}^{N} V_k\xi_k\right)\frac{\partial\xi_k}{\partial Y}\right]\xi_i dXdY \\ &+ \gamma\left[\sum_{k=1}^{N} U_k\int \frac{\partial\xi_i}{\partial X}\frac{\partial\xi_k}{\partial X}dXdY + \sum_{k=1}^{N} V_k\int \frac{\partial\xi_i}{\partial X}\frac{\partial\xi_k}{\partial Y}dXdY\right] \\ &+ Pr\sum_{k=1}^{N} U_k\int\left[\frac{\partial\xi_i}{\partial X}\frac{\partial\xi_k}{\partial X} + \frac{\partial\xi_i}{\partial Y}\frac{\partial\xi_k}{\partial Y}\right]dXdY + PrHa^2H_Y^2\int\left(\sum_{k=1}^{N} U_k\xi_k\right)\xi_i dXdY \\ &- PrHa^2H_XH_Y\int\left(\sum_{k=1}^{N} V_k\xi_k\right)\xi_i dXdY \end{aligned} \tag{25}$$

$$\begin{aligned} R_i^2 \approx{}& \sum_{k=1}^{N} V_k \int \frac{\partial\xi_k}{\partial Fo}\xi_i dXdY + \sum_{k=1}^{N} V_k \int \left[\left(\sum_{k=1}^{N} U_k\xi_k\right)\frac{\partial\xi_k}{\partial X} + \left(\sum_{k=1}^{N} V_k\xi_k\right)\frac{\partial\xi_k}{\partial Y}\right]\xi_i dXdY \\ &+ \gamma\left[\sum_{k=1}^{N} U_k\int \frac{\partial\xi_i}{\partial Y}\frac{\partial\xi_k}{\partial X}dXdY + \sum_{k=1}^{N} V_k\int \frac{\partial\xi_i}{\partial Y}\frac{\partial\xi_k}{\partial Y}dXdY\right] \end{aligned}$$

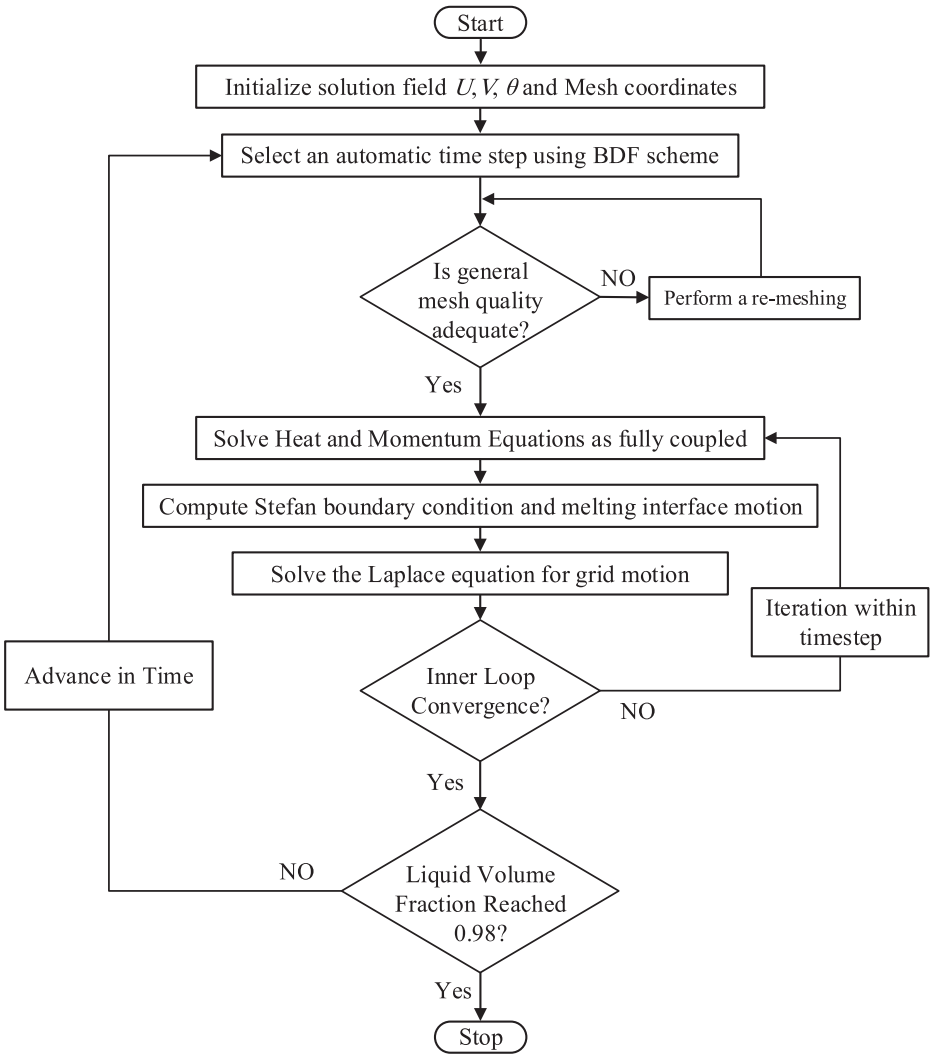

Fig. 2. Flowchart of the utilized numerical approach.

$$+ Pr\sum_{k=1}^{N} V_k \int \left[\frac{\partial \xi_i}{\partial X}\frac{\partial \xi_k}{\partial X} + \frac{\partial \xi_i}{\partial Y}\frac{\partial \xi_k}{\partial Y}\right] dXdY - RaPr \int \left(\sum_{k=1}^{N} \theta_k \xi_k\right) \xi_i dXdY$$
$$+ PrHa^2 H_X^2 \int \left(\sum_{k=1}^{N} V_k \xi_k\right) \xi_i dXdY - PrHa^2 H_X H_Y \int \left(\sum_{k=1}^{N} U_k \xi_k\right) \xi_i dXdY \quad (26)$$

$$R_i^3 \approx \sum_{k=1}^{N} \theta_k \int \frac{\partial \xi_k}{\partial Fo} \xi_i dXdY + \sum_{k=1}^{N} \theta_k \int \left[\left(\sum_{k=1}^{N} U_k \xi_k\right)\frac{\partial \xi_k}{\partial X} + \left(\sum_{k=1}^{N} V_k \xi_k\right)\frac{\partial \xi_k}{\partial Y}\right] \xi_i dXdY$$
$$+ \sum_{k=1}^{N} \theta_k \int \left[\frac{\partial \xi_i}{\partial X}\frac{\partial \xi_k}{\partial X} + \frac{\partial \xi_i}{\partial Y}\frac{\partial \xi_k}{\partial Y}\right] dXdY - EcHa^2 \left(H_Y \int \left[\sum_{k=1}^{N} U_k \xi_k\right] - H_X \int \left[\sum_{k=1}^{N} V_k \xi_k\right]\right)^2 \xi_i dXdY \quad (27)$$

The Laplace equation was utilized to compute the grid motion. The motion of the phase change interface was controlled using the Stefan boundary condition. The motion of the vertical walls was fixed in a horizontal direction, but they were allowed to move in the vertical direction. In the same way, the motion of the horizontal walls was fixed in the vertical direction, but they were allowed to move in the horizontal direction. The fixed boundary conditions for horizontal and vertical walls forces the cavity to remain in its original form, but it also provides enough flexibility for the grid to move smoothly. A systematic re-meshing based on the general mesh quality is also employed to ensure the quality of the grid.

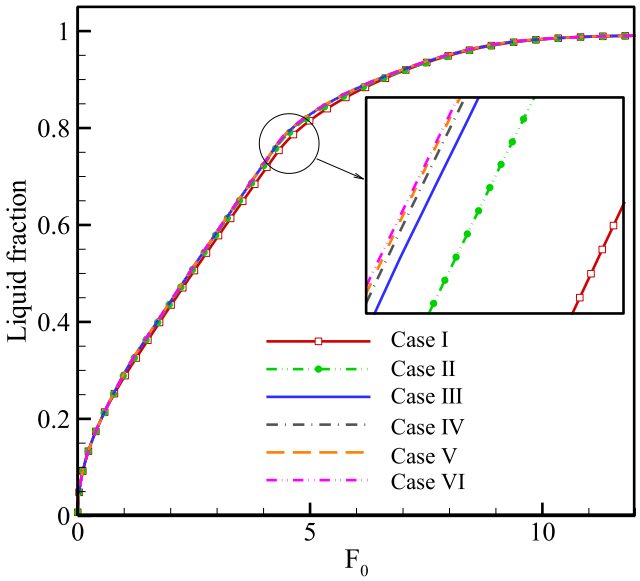

Fig. 3. The dependency of the liquid fraction on the grid size.

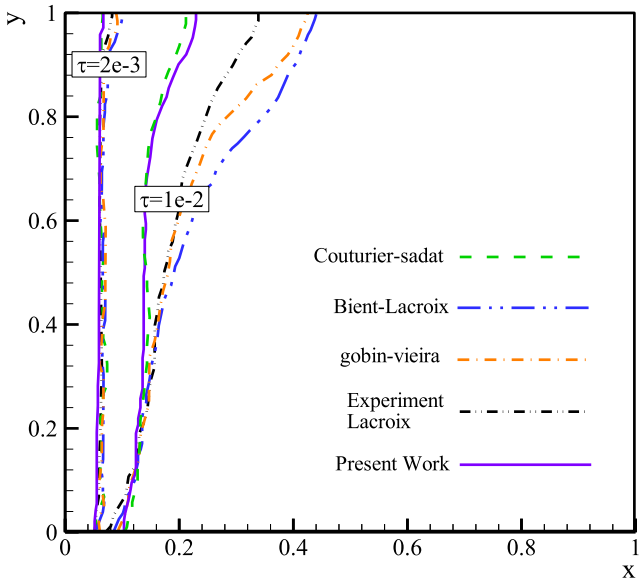

Fig. 4. Comparison between the results of current work and those reported in Bertrand et al. [52].

The solution from the previous mesh was interpolated into the new mesh. The time step is automatically controlled using the Backward Differentiation Formula (BDF). The time step selected based on a free time steps scheme within BFD order in the range of one and two [50]. The following chart representing the algorithm of the numerical approach is depicted in Fig. 2.

3.1. Grid test and verification

In the numerical calculations, the study of grid independence is momentous so that the study is incomplete without doing this operation. For this purpose, the computational domain is divided into two regions: the melted liquid and the solid substances. A structured mesh with quadratic elements is used to discretize the melted liquid region while another region is discretized by employing unstructured mesh and triangular elements. The number of elements for both the liquid and solid regions is presented Table 1 for $Ra = 2.1 \times 10^5$, $Pr = 0.021$, $Ste = 0.039$, $Ha = 10$, $Y_0 = 0.5$, $Ec = 10^{-6}$. The liquid fraction, corresponding to various grid sizes of Table 1, is plotted in Fig. 3. It is observed that case III provides accurate results for the solution.

Table 1
The grid sizes in the liquid and the solid regions.

Cases	Case I	Case II	Case III	Case IV	Case V	Case VI
Grid size in solid	183	686	974	1597	1941	2275
Grid size in liquid	20×20	40×40	60×60	80×80	100×100	120×120

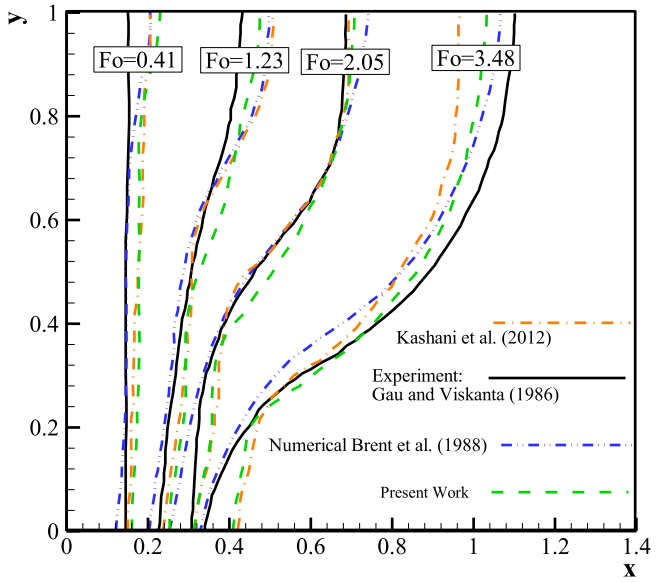

Fig. 5. Comparison between the results of current work and those reported in literature [53].

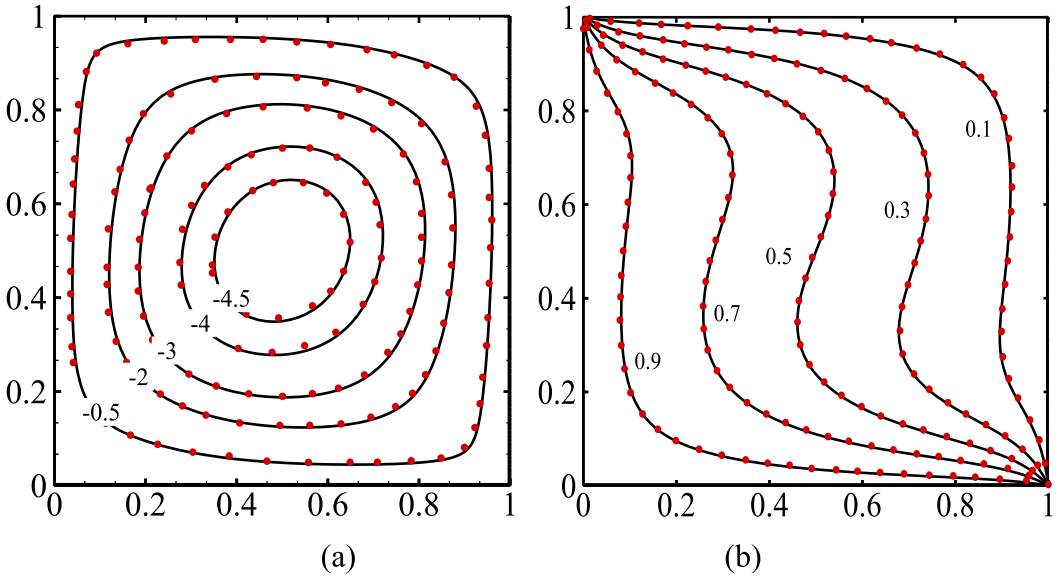

Fig. 6. Comparison between (a): streamlines and (b): isotherms of the current work (solid lines) and those reported (points) in Sathiyamoorthy and Chamkha [47].

The accuracy and correctness of the utilized code are evaluated by comparing the outcomes of the present work and those mentioned in [35,47,51–53]. Figs. 4–7 show these verifications and validations. The results show excellent accommodations between the outcomes of the present study and previous works.

Figs. 4 and 5 depict admissible agreement with the results of the current work and those reported in the literature. The main reason for the discrepancies between the results is the fact that the phase change occurs at a fixed fusion temperature; however, using a fixed fusion temperature results in a discontinuity in the heat equation. Therefore, in the enthalpy-porosity

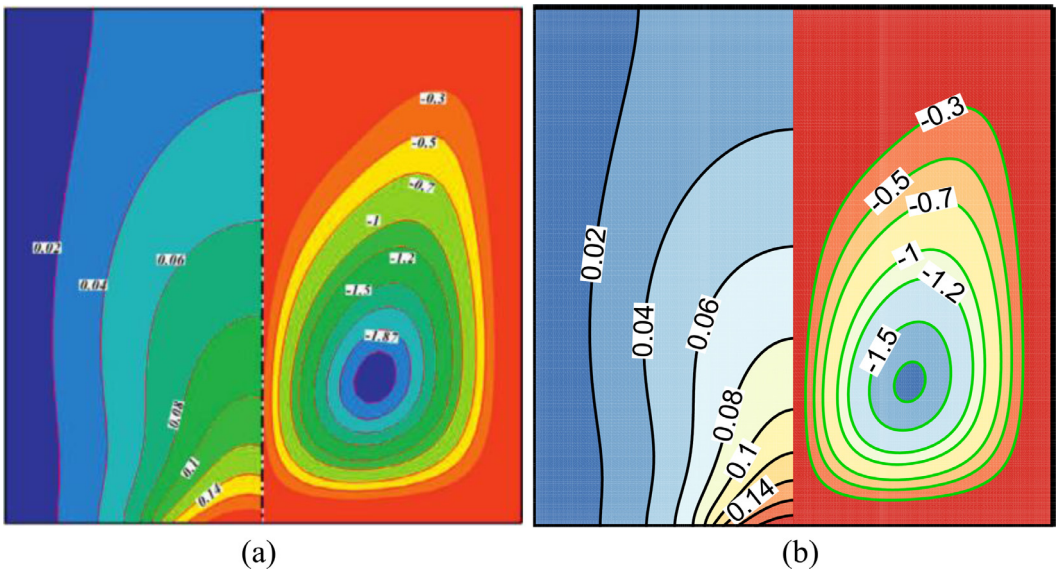

Fig. 7. Temperature and streamlines of the work done by (a): Sheikholeslami and Vajravelu [35] and (b): the current work.

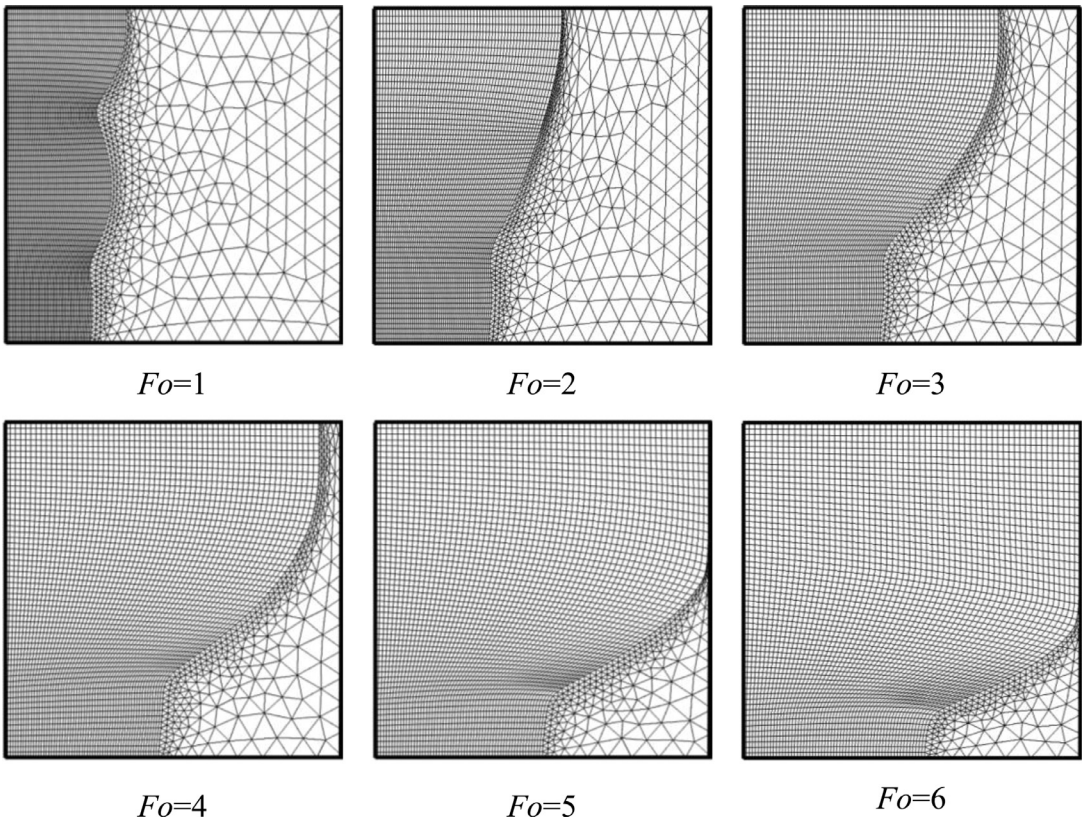

Fig. 8. Display of the deformable mesh during the melting process.

method, the fusion occurs in a narrow temperature range. Capturing accurate fusion interface requires a narrow band of $\delta\theta$ and a large value of A_{mush} parameter. However, employing a narrow band of $\delta\theta$ and a large value of A_{mush} significantly reduced the stability of the governing equation. Using a narrow band for fusion temperature demands a very fine grid. To reduce the computational cost, some researchers have used a larger fusion temperature and a small value of A_{mush}. Therefore, the phase change interface reported by various researchers is not unique. In the present study, we utilized a new approach based on the deformed grid method, in which the phase change occurs at the exact fusion temperature

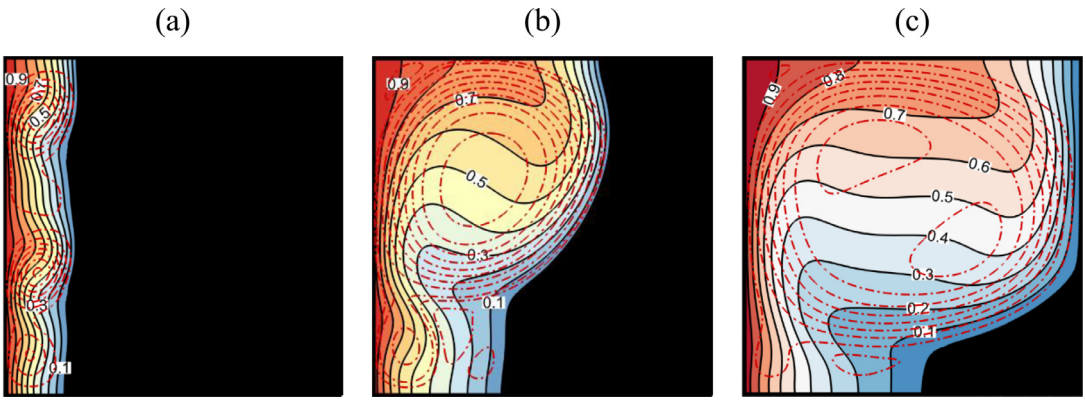

Fig. 9. Display of streamlines and isotherms for Ha=0 and $Y_0 = 0.5$ when Fourier number (Fo) is: (a): 0.5, (b): 2.5 and (c): 5.

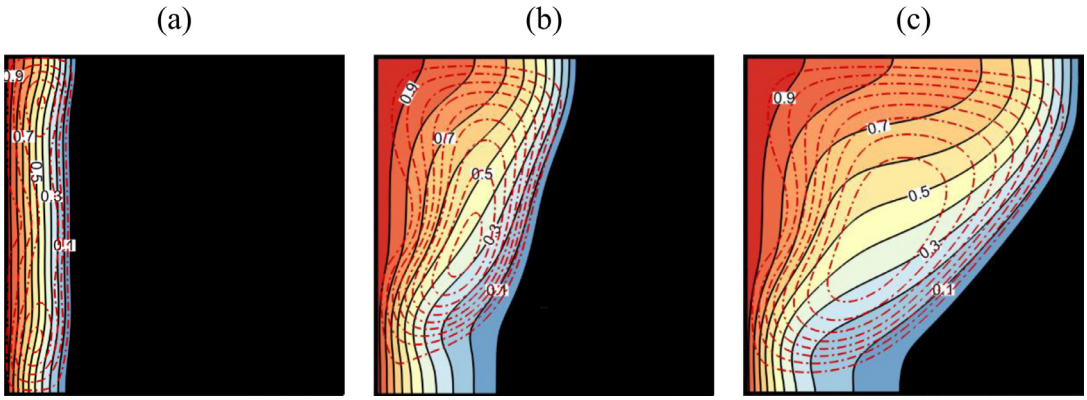

Fig. 10. Display of streamlines and isotherms for Ha=25 and Y_0=0.5 when Fourier number (Fo) is: (a): 0.5, (b): 2.5 and (c): 5.

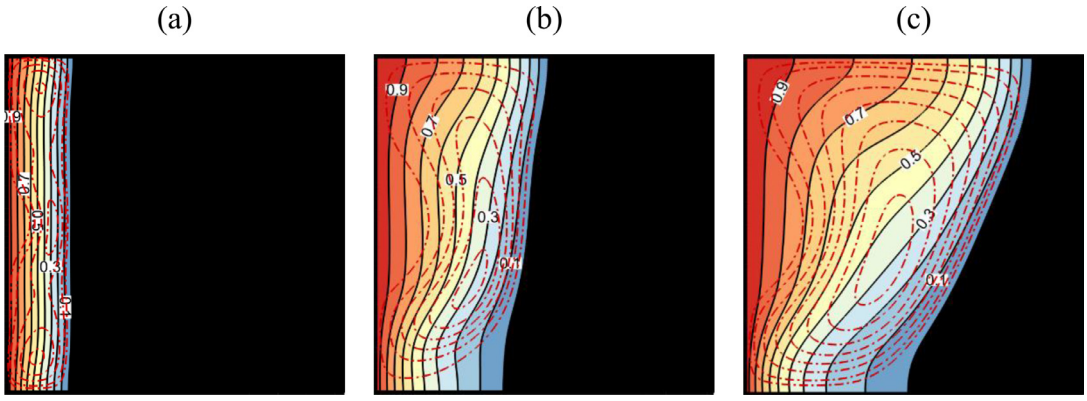

Fig. 11. Display of streamlines and isotherms for $Ha = 50$ and $Y_0 = 0.5$ when Fourier number (Fo) is: (a): 0.5, (b): 2.5 and (c): 5.

with no need of using a phase change temperature band. Moreover, most of the experimental works have used mechanical methods to capture the phase change interface. For instance, Gau and Viskanta [53] utilized a mechanical probe to capture the melting interface. At the onset of phase change, the melting interface is unstable, and the measurement of the phase change interface using mechanical probes involves some degrees of deviation.

4. Results and discussion

This work aims to study the existence effects of the non-uniform magnetic field on the melting process driven by the natural convection. The impacts of strength ($0 \leq Ha \leq 50$) and location ($0 \leq Y_0 \leq 1$) of the magnetic field on the mass

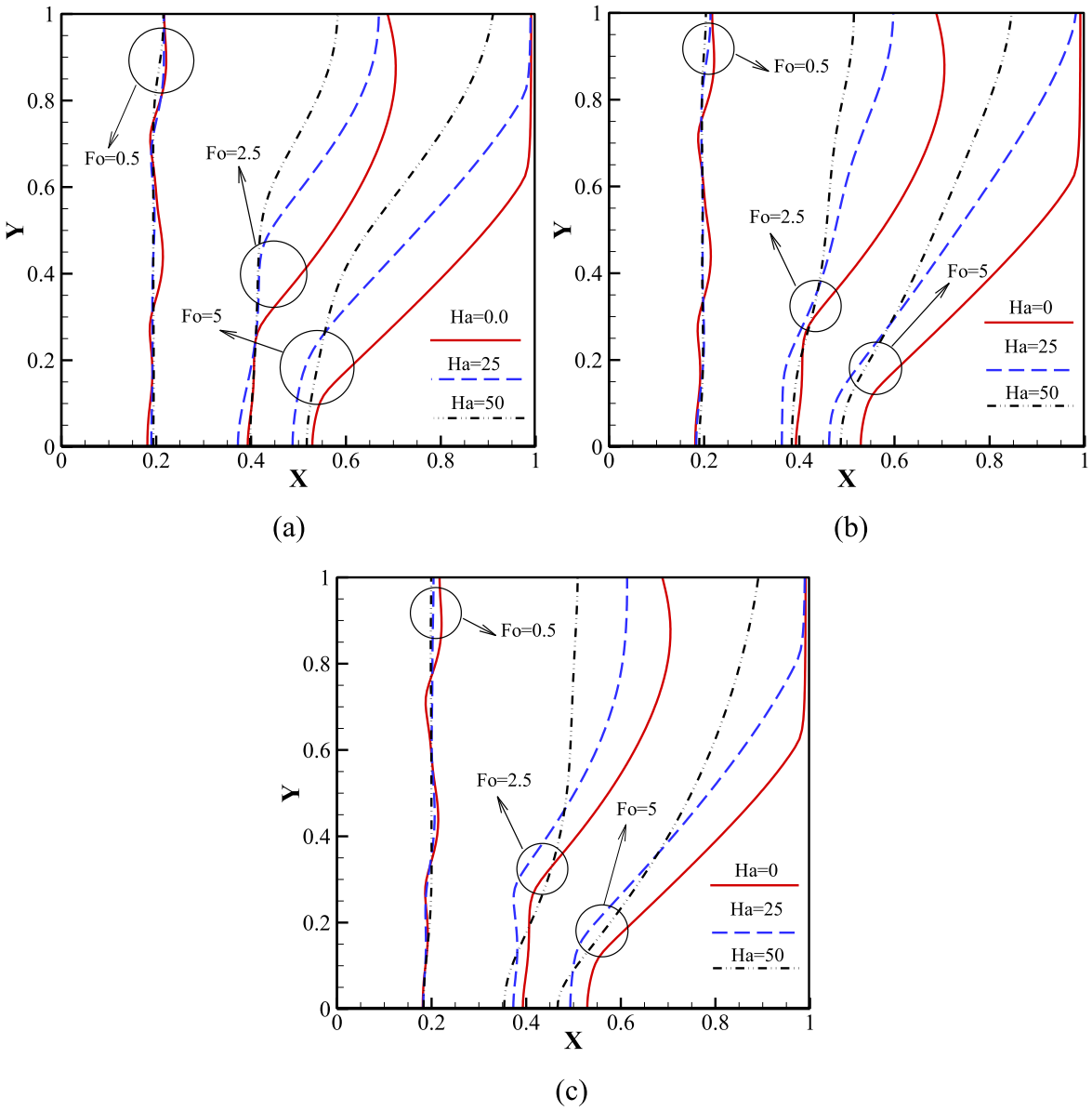

Fig. 12. Melting front surface for various Hartman and Fourier numbers at different locations of the magnetic source: (a): $Y_0 = 0.0$, (b): $Y_0 = 0.5$ and (c): $Y_0 = 1.0$.

fraction of the melted liquid are perused while the other parameters are kept constant so that $Ra = 2.1 \times 10^5$, $Pr = 0.021$, $Ste = 0.039$ and $Ec = 10^{-6}$.

Fig. 8 depicts the deformable grid patterns during the melting process for various Fourier number when $Ha = 30$ and $Y_0 = 0.5$. As depicted, the structured and unstructured grids are used to discretizing melted fluid and solid substances, respectively. It is worth mentioning that the employed code utilizes the re-meshing technique during melting progress to satisfy the accuracy of the results. As seen in this figure, a large grid-size is utilized in the solid region because there is no significant temperature gradient in the solid region. Moreover, the temperature of the interface and the cold wall are equal in solid region, and hence, the non-dimensional temperature in the solid domain is zero (Fig. 8).

Figs. 9–11 depict the melting front surface, streamlines and isotherms patterns of the melted liquid for the different Fourier and Hartman numbers when $Y_0 = 0.5$. Increasing Fourier number develops the melted liquid region and the depth of the melting-front surface. It is obvious that an increase in Hartman number Ha descends the melted liquid space. The Lorenz force is acting as a resistance force and decreases the strength of the convection mechanism in the melting region, and hence, the increment of Hartman number descends the rate of melting. Additionally, the force of the magnetic source acts as a strong barrier for fluid motion next to the hot wall. However, the strength of the magnetic force drastically decreases

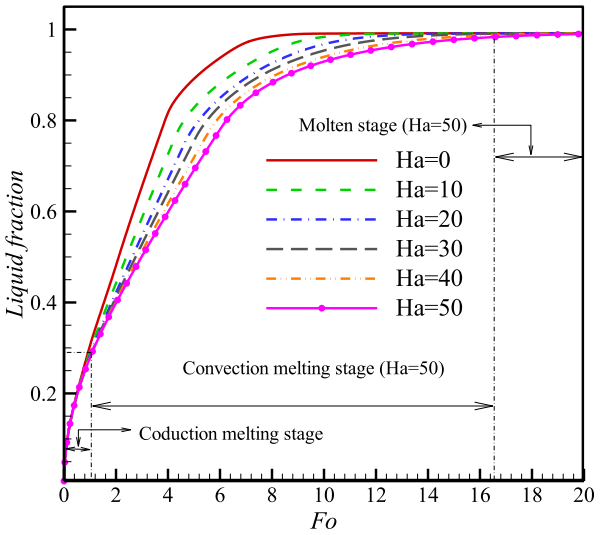

Fig. 13. Liquid fraction as a function of Fourier number *Fo* for different Hartman numbers *Ha*.

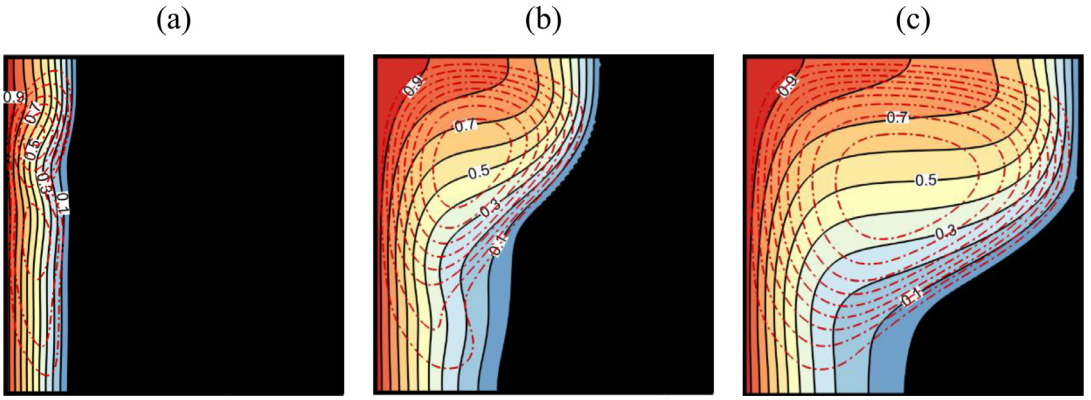

Fig. 14. Display of streamlines and isotherms for $Y_0 = 0.0$, $Ha = 25$ when Fourier number (*Fo*) is: (a): 0.5, (b): 2.5 and (c): 5.

as the distance between the magnetic source and the fluid increases. This phenomenon can decline the convection heat transfer from the hot wall.

The impact of the Hartman number (*Ha*) on the melting process is studied using the melting-front surfaces. Here, the melting-front surfaces are depicted as curves in 2D. Fig. 12 shows the melting-front surfaces. When Fo=0.5, the variation of Hartman number does not show a significant effect on the melted liquid space. However, the effect of Hartman number on the melting front progress is notable when the Fourier number is high. The reason is that a direct relationship exists between the Lorentz force and the melted liquid velocity. Indeed, when the molten fraction is low, the motion of the fluid is bounded by the zero velocity at nearby walls. By the increase of Fourier number, the melted region expands, and the fluid has more freedom to move.

Fig. 13 depicts the effects of Hartman number on the liquid fraction as a function of the Fourier number when Y_0=0.5. As depicted, when *Fo* is less than 1.15, it can be said that Hartman number does not induce a notable effect on the melted liquid fraction. This is because the Lorentz force is entirely dependent on the velocity. At this stage, the velocities are very low (near to zero), and hence, the conduction heat transfer is dominant, this is the first stage which known as the conduction melting zone. The second stage in the process is dominated by heat convection melting and is utterly dependent on the Hartman number. The convection stage of melting lasts longer at higher *Ha*. This means that the increment of *Ha* decreases melted liquid fraction.

Figs. 14–16 depicts the impacts of the magnetic source locations on the melting process at various Fourier numbers. As can be seen in Figs. 14–16, the magnetic source location does not show a notable effect on the melted liquid space and the depth of melting front for $Fo = 0.5$; however, the streamlines patterns are entirely affected by the source location. Additionally, it can be seen that the source location significantly impresses the depth of the melting front for further Fourier numbers. As previously mentioned, the force arising from the magnetic field depends on the velocity magnitude, and hence, the effectiveness of the source location is more evident at the higher Fourier numbers.

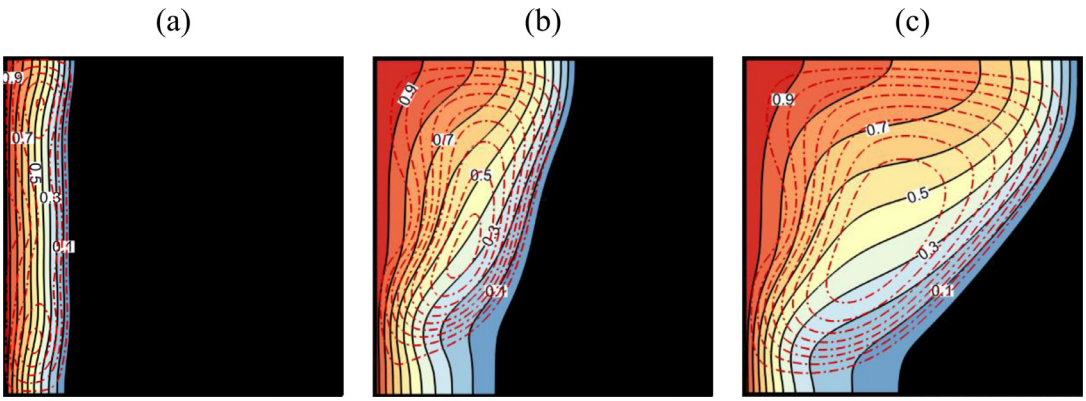

Fig. 15. Display of streamlines and isotherms for $Y_0 = 0.5$, $Ha = 25$ when Fourier number (Fo) is: (a): 0.5, (b): 2.5 and (c): 5.

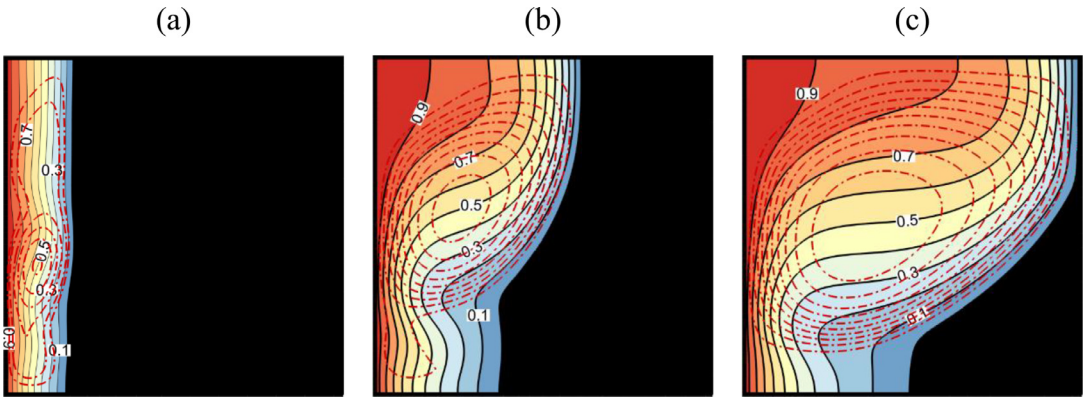

Fig. 16. Display of streamlines and isotherms for $Y_0 = 1.0$, $Ha = 25$ when Fourier number (Fo) is: (a): 0.5, (b): 2.5 and (c): 5.

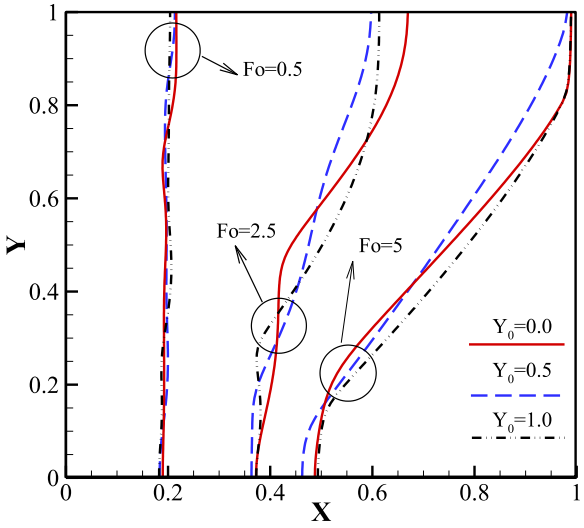

Fig. 17. Melting front surface for different locations of the magnetic source when Ha=25.

The melting-front surfaces for the different values of Fourier number and the magnetic source locations are shown in Fig. 17 to demonstrate the effects of the source location on the melting front progress. Once again, when Fo=0.5, the effect of the increase of Hartman number on the melted liquid space is not notable. However, the effect of Hartman number on the melting front progress is significant when Fourier number is high. The reason is that there exists a direct relationship between the Lorentz force and the melted liquid velocity increasing with Fourier number. Considering Fo=2.5, when the

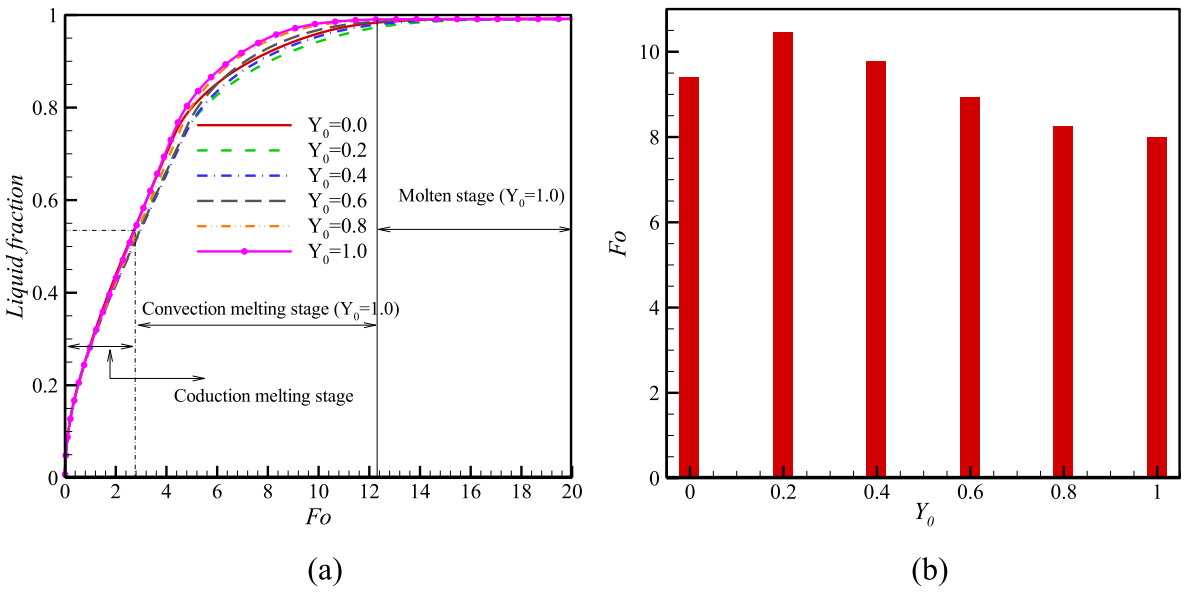

Fig. 18. Melting fraction and required time; (a): Liquid fraction as a function of *Fo* and (b): The time required to complete melting for different values of Y_0.

magnetic source is located next to the bottom of the cavity, the below parts of the melting interface are under the significant influence of the magnetic force, and hence, the melting interface from Y_0=0 to Y_0=0.5 is almost a straight line which shows a conduction-dominant mechanism. Relocating the magnetic source to the middle and top of the cavity reduces the effect of the magnetic on the downside parts of the melting interface. When the magnetic source is at the bottom of the cavity, the top parts of the interface are in a large distance from the magnetic source, and hence, the fluid would experience a lower magnetic resistant force at the top parts of the cavity. Hence, the fluid velocity increases and the convection mechanism enhances in this zone. As a result, the top part of the melting interface is further advanced in the solid zone, $X \sim 0.6$. In contrast, when the magnetic source is in the middle or top of the cavity, the fluid would experience a large magnetic force, and as a result, the convection heat transfer reduces. As seen, in this case, the top section of the melting interface is located at $X \sim 0.5$.

Fig. 18(a) depicts the effects of source magnetic location on the liquid fraction as a function of Fourier number for *Ha*=25. As shown, when *Fo* is less than 2.8, the source location does not alter the melted liquid fraction. As previously mentioned, the first stage is dominated by heat conduction melting. In the convection stage of melting and for *Y*0<0.4, there is not a specific trend as Y_0 approaches 0.4. Whereas, when Y_0>0.4, an increment of Y_0 increases the liquid fraction. Moreover, Fig. 18(b) illustrates that the required time for full melting is the highest when Y_0=0.2. However, the required full melting time is the lowest when the source is located at Y_0=1.0. It worth noting that the liquid fraction of 0.98 is considered as the criterion in which the PCM is fully melted.

5. Conclusion

The melting flow and heat transfer in a cavity under the influence of a line-source magnetic field was addressed in this work. The cavity was divided into two domains of liquid and solid PCMs. The governing equations in the melting (liquid) part of the cavity were fluid continuity, the laminar momentum equations, and the heat equation. The governing equation in the solid domain was solely the heat transfer in solids. The phase change effect was introduced at the interface of the liquid and solid domains by considering a constant fusion temperature at the interface. Then, the displacement of the interface was linked to the heat transfer at the domain interface based on interfacial energy balance. The difference of energies reaching the interface from the liquid and solid domains resulted in the phase change and displacement of the interface (Stefan condition). The governing equations were transformed in a non-dimensional form to generalize the solutions. The finite element method associated with ALE moving grid technique was utilized to solve the governing equations. The grid check was performed, and the results in some limited cases were compared with the available literature and found in good agreement. The effect of the magnitude of the magnetic field and the magnetic source location on the melting behavior of PCMs were investigated. The outcomes can be summarized as follows:

1- The moving grid technique is capable of handling phase change heat transfer in a square enclosure.
2- The magnitude and location of the magnetic field source do not show a significant effect on the natural convection heat transfer at the initial melting times, but with the advancement of the melting-front and the increase of the melt volume fraction, the velocity of the fluid increases and the effect of magnetic field boosts.

3- The magnetic field tends to suppress the natural convective flows and make the melting interface uniform. The location of the magnetic source can affect the shape of the melting front.

By utilizing a uniform magnetic field, the control of the melting interface is only possible by suppressing the natural convection in the entire liquid domain. In contrast, the non-uniform magnetic field provides a good way of adjusting the location of the magnetic source for controlling the melting process. The focus of the present study was the analysis of the melting process subject to a non-uniform magnetic field; however, the solidification process is also essential in the design of PCM containers and metal casting. Hence, analysis of solidification of PCMs subject to the variable point-source magnetic field can be subject of future studies.

Acknowledgments

This work of Mohammad Ghalambaz was supported by the STAR Institute - UBB, Cluj-Napoca, Romania, External Fellowship program, and the work by Ioan Pop has been supported from the Grant PN-III-P4-IDPCE- 2016-0036, UEFISCDI, Romanian Ministry of Sciences. Dongsheng Wen acknowledge the support from National Science Foundation of China (No. 51876006), National Numerical Windtunnel (Grant 2018-ZT3A05) and 111 projects (B18002). The authors wish to express their thanks to the very competent Reviewers for the excellent comments and suggestions.

Supplementary material

Supplementary material associated with this article can be found, in the online version, at doi:10.1016/j.apm.2019.09.015.

References

[1] R. Baetens, B.P. Jelle, A. Gustavsen, Phase change materials for building applications: a state-of-the-art review, Energy Build. 42 (9) (2010) 1361–1368.
[2] H. Akeiber, et al., A review on phase change material (PCM) for sustainable passive cooling in building envelopes, Renew. Sustain. Energy Rev. 60 (2016) 1470–1497.
[3] B. Xu, P. Li, C. Chan, Application of phase change materials for thermal energy storage in concentrated solar thermal power plants: a review to recent developments, Appl. Energy 160 (2015) 286–307.
[4] M. Sheikholeslami, R.-u. Haq, A. Shafee, Z. Li, Heat transfer behavior of nanoparticle enhanced pcm solidification through an enclosure with v shaped fins, Int. J. Heat Mass Transf. 130 (2019) 1322–1342.
[5] M. Sheikholeslami, R.-u. Haq, A. Shafee, Z. Li, Y.G. Elaraki, I. Tlili, Heat transfer simulation of heat storage unit with nanoparticles and fins through a heat exchanger, Int. J. Heat Mass Transf. 135 (2019) 470–478.
[6] M. Sheikholeslami, O. Mahian, Enhancement of pcm solidification using inorganic nanoparticles and an external magnetic field with application in energy storage systems, J. Clean. Prod. 215 (2019) 963–977.
[7] M. Sheikholeslami, M. Jafaryar, A. Shafee, Z. Li, Simulation of nanoparticles application for expediting melting of pcm inside a finned enclosure, Phys. A: Stat. Mech. Appl. 523 (2019) 544–556.
[8] S. Farah, H. Farouk, Phase change materials (PCM) for cooling applications in buildings, Energy Build. 129 (2016) 396–431.
[9] P.A. Fokaides, A. Kylili, S.A. Kalogirou, Phase change materials (PCMs) integrated into transparent building elements: a review, Mater. Renew. Sustain. Energy 4 (2) (2015) 6.
[10] T. Silva, R. Vicente, F. Rodrigues, Literature review on the use of phase change materials in glazing and shading solutions, Renew. Sustain. Energy Rev. 53 (2016) 515–535.
[11] N. Tay, M. Liu, M. Belusko, F. Bruno, Review on transportable phase change material in thermal energy storage systems, Renew. Sustain. Energy Rev. 75 (2017) 264–277.
[12] M. Malik, I. Dincer, M.A. Rosen, Review on use of phase change materials in battery thermal management for electric and hybrid electric vehicles, Int. J. Energy Res. 40 (8) (2016) 1011–1031.
[13] S. Chandel, T. Agarwal, Review of cooling techniques using phase change materials for enhancing efficiency of photovoltaic power systems, Renew. Sustain. Energy Rev. 73 (2017) 1342–1351.
[14] A. Kylili, P.A. Fokaides, Numerical simulation of phase change materials for building applications: a review, Adv. Build. Energy Res. 11 (1) (2017) 1–25.
[15] A.I. Alsabery, I. Hashim, A.J. Chamkha, H. Saleh, B. Chanane, Effect of spatial side-wall temperature variation on transient natural convection of a nanofluid in a trapezoidal cavity, Int. J. Numer. Methods Heat Fluid Flow 27 (6) (2017) 1365–1384.
[16] A.I. Alsabery, R. Mohebbi, A.J. Chamkha, I. Hashim, Effect of local thermal non-equilibrium model on natural convection in a nanofluid-filled wavy-walled porous cavity containing inner solid cylinder, Chem. Eng. Sci. 201 (2019) 247–263 2019/06/29/.
[17] K. Janagi, S. Sivasankaran, M. Bhuvaneswari, M. Eswaramurthi, Numerical study on free convection of cold water in a square porous cavity heated with sinusoidal wall temperature, Int. J. Numer. Methods Heat Fluid Flow 27 (4) (2017) 1000–1014.
[18] I. Pop, M. Sheremet, D.S. Cimpean, Natural convection in a partially heated wavy cavity filled with a nanofluid using buongiorno's nanofluid model, Int. J. Numer. Methods Heat Fluid Flow 27 (4) (2017) 924–940.
[19] H. Zargartalebi, M. Ghalambaz, A. Chamkha, I. Pop, A.S. Nezhad, Fluid-structure interaction analysis of buoyancy-driven fluid and heat transfer through an enclosure with a flexible thin partition, Int. J. Numer. Methods Heat Fluid Flow 28 (9) (2018) 2072–2088.
[20] M. Sheikholeslami, Numerical approach for mhd Al_2O_3-water nanofluid transportation inside a permeable medium using innovative computer method, Comput. Methods Appl. Mech. Eng. 344 (2019) 306–318.
[21] M. Sheikholeslami, New computational approach for exergy and entropy analysis of nanofluid under the impact of lorentz force through a porous media, Comput. Methods Appl. Mech. Eng. 344 (2019) 319–333.
[22] A. Rashad, T. Armaghani, A. Chamkha, M. Mansour, Entropy generation and mhd natural convection of a nanofluid in an inclined square porous cavity: effects of a heat sink and source size and location, Chin. J. Phys. 56 (1) (2018) 193–211.
[23] A. Dogonchi, T. Armaghani, A.J. Chamkha, D. Ganji, Natural convection analysis in a cavity with an inclined elliptical heater subject to shape factor of nanoparticles and magnetic field, Arab. J. Sci. Eng. 44 (9) (2019) 7919–7931.
[24] A. Dogonchi, T. Tayebi, A.J. Chamkha, and D. Ganji, Natural convection analysis in a square enclosure with a wavy circular heater under magnetic field and nanoparticles, J. Therm. Anal. Calorim., pp. 1–11, doi:10.1007/s10973-019-08408-0.
[25] A. Chamkha, F. Selimefendigil, MHD free convection and entropy generation in a corrugated cavity filled with a porous medium saturated with nanofluids, Entropy 20 (11) (2018) 846.
[26] M.A. Sheremet, M.S. Astanina, I. Pop, MHD natural convection in a square porous cavity filled with a water-based magnetic fluid in the presence of geothermal viscosity, Int. J. Numer. Methods Heat Fluid Flow 28 (9) (2018) 2111–2131.

[27] N. Reddy, K. Murugesan, Magnetic field influence on double-diffusive natural convection in a square cavity – a numerical study, Numer. Heat Transf. Part A: Appl. 71 (4) (2017) 448–475.
[28] N.S. Bondareva, M.A. Sheremet, Effect of inclined magnetic field on natural convection melting in a square cavity with a local heat source, J. Magn. Magn. Mater. 419 (2016) 476–484.
[29] N.S. Bondareva, M.A. Sheremet, Natural convection heat transfer combined with melting process in a cubical cavity under the effects of uniform inclined magnetic field and local heat source, Int. J. Heat Mass Transf. 108 (2017) 1057–1067.
[30] M. Sheikholeslami, H.B. Rokni, Melting heat transfer influence on nanofluid flow inside a cavity in existence of magnetic field, Int. J. Heat Mass Transf. 114 (2017) 517–526.
[31] M. Sheikholeslami, D.D. Ganji, M.M. Rashidi, Ferrofluid flow and heat transfer in a semi annulus enclosure in the presence of magnetic source considering thermal radiation, J. Taiwan Inst. Chem. Eng. 47 (2015) 6–17.
[32] M. Sheikholeslami, M. Rashidi, D. Ganji, Effect of non-uniform magnetic field on forced convection heat transfer of Fe_3O_4–water nanofluid, Comput. Methods Appl. Mech. Eng. 294 (2015) 299–312.
[33] M. Sheikholeslami, M.M. Rashidi, Effect of space dependent magnetic field on free convection of Fe_3O_4–water nanofluid, J. Taiwan Inst. Chem. Eng. 56 (2015) 6–15 2015/11/01/.
[34] M. Sheikholeslami, S.A.M. Mehryan, A. Shafee, M.A. Sheremet, Variable magnetic forces impact on magnetizable hybrid nanofluid heat transfer through a circular cavity, J. Mol. Liq. 277 (2019) 388–396 2019/03/01/.
[35] M. Sheikholeslami, K. Vajravelu, Nanofluid flow and heat transfer in a cavity with variable magnetic field, Appl. Math. Comput. 298 (2017) 272–282.
[36] M. Sheikholeslami, M.B. Gerdroodbary, D. Ganji, Numerical investigation of forced convective heat transfer of Fe3O4-water nanofluid in the presence of external magnetic source, Comput. Methods Appl. Mech. Eng. 315 (2017) 831–845.
[37] M. Sheikholeslami, Magnetic source impact on nanofluid heat transfer using cvfem, Neural Comput. Appl. 30 (4) (2018) 1055–1064.
[38] R. Viswanath, Y. Jaluria, A comparison of different solution methodologies for melting and solidification problems in enclosures, Numer. Heat Transf. Part B Fundam. 24 (1) (1993) 77–105.
[39] I. Wintruff, C. Günther, A. Class, An interface-tracking control-volume finite-element method for melting and solidification problems. Part I: formulation, Numer. Heat Transf.: Part B: Fundam. 39 (2) (2001) 101–125.
[40] C.-Y. Li, S.V. Garimella, J.E. Simpson, Fixed-grid front-tracking algorithm for solidification problems. Part I: method and validation, Numer. Heat Transf. Part B: Fundam. 43 (2) (2003) 117–141.
[41] B. Sushobhan, S. Kar, Thermal modeling of melting of nano based phase change material for improvement of thermal energy storage, Energy Procedia 109 (2017) 385–392.
[42] X.-H. Yang, S.-C. Tan, J. Liu, Numerical investigation of the phase change process of low melting point metal, Int. J. Heat Mass Transf. 100 (2016) 899–907.
[43] W.-B. Ye, Melting process in a rectangular thermal storage cavity heated from vertical walls, J. Therm. Anal. Calorim. 123 (1) (2016) 873–880.
[44] R. Hossain, S. Mahmud, A. Dutta, I. Pop, Energy storage system based on nanoparticle-enhanced phase change material inside porous medium, Int. J. Therm. Sci. 91 (2015) 49–58.
[45] M.S. Al-Jethelah, S.H. Tasnim, S. Mahmud, A. Dutta, Melting of nano-phase change material inside a porous enclosure, Int. J. Heat Mass Transf. 102 (2016) 773–787.
[46] , The finite element method for fluid dynamics, in: O.C. Zienkiewicz, R.L. Taylor, P. Nithiarasu (Eds.), The Finite Element Method for Fluid Dynamics, Seventh ed., Butterworth-Heinemann, Oxford, 2014, p. iii.
[47] M. Sathiyamoorthy, A. Chamkha, Effect of magnetic field on natural convection flow in a liquid gallium filled square cavity for linearly heated side wall (s), Int. J. Therm. Sci. 49 (9) (2010) 1856–1865.
[48] P.R. Amestoy, I.S. Duff, J.-Y. L'excellent, Multifrontal parallel distributed symmetric and unsymmetric solvers, Comput. Methods Appl. Mech. Eng. 184 (2–4) (2000) 501–520.
[49] P.R. Amestoy, A. Guermouche, J.-Y. L'Excellent, S. Pralet, Hybrid scheduling for the parallel solution of linear systems, Parallel Comput. 32 (2) (2006) 136–156.
[50] J.C. De Los Reyes, S. González Andrade, A combined BDF-semismooth Newton approach for time-dependent bingham flow, Numer. Methods Partial Differ. Equ. 28 (3) (2012) 834–860.
[51] S. Kashani, A. Ranjbar, M. Abdollahzadeh, S. Sebti, Solidification of nano-enhanced phase change material (NEPCM) in a wavy cavity, Heat Mass Transf. 48 (7) (2012) 1155–1166.
[52] O. Bertrand, et al., Melting driven by natural convection a comparison exercise: first results, Int. J. Therm. Sci. 38 (1) (1999) 5–26.
[53] C. Gau, R. Viskanta, Melting and solidification of a pure metal on a vertical wall, J. Heat Transf. 108 (1) (1986) 174–181.